Infection, Genetics and Evolution 102 (2022) 105310

Contents lists available at ScienceDirect

Infection, Genetics and Evolution

journal homepage: www.elsevier.com/locate/meegid

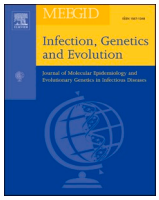

# Designing potential siRNA molecules for silencing the gene of the nucleocapsid protein of Nipah virus: A computational investigation

AMUB Mahfuz [a], Md. Arif Khan [a,f,*], Emran Hossain Sajib [b], Anamika Deb [c], Shafi Mahmud [d], Mahmudul Hasan [b,c], Otun Saha [e], Ariful Islam [f,h], Md. Mizanur Rahaman [g,**]

[a] Department of Biotechnology and Genetic Engineering, University of Development Alternative, Dhaka 1209, Bangladesh
[b] Faculty of Biotechnology and Genetic Engineering, Sylhet Agricultural University, Sylhet 3100, Bangladesh
[c] Department of Pharmaceuticals and Industrial Biotechnology, Faculty of Biotechnology and Genetic Engineering, Sylhet Agricultural University, Sylhet 3100, Bangladesh
[d] Microbiology Laboratory, Bioinformatics Division, Department of Genetic Engineering and Biotechnology, University of Rajshahi, Rajshahi 6205, Bangladesh
[e] Department of Microbiology, Noakhali Science and Technology University, Noakhali 3814, Bangladesh
[f] Institute of Epidemiology, Disease Control and Research (IEDCR), Dhaka 1212, Bangladesh
[g] Department of Microbiology, University of Dhaka, Dhaka, Bangladesh
[h] EcoHealth Alliance, New York, NY 10018, USA

ARTICLE INFO

*Keywords:*
Nipah virus
Nucleocapsid protein gene
siRNA
Evolutionary analysis
Encephalitis
Viral pneumonia

ABSTRACT

Nipah virus (NiV), a zoonotic virus, engenders severe infections with noticeable complications and deaths in humans and animals. Since its emergence, it is frightening, this virus has been causing regular outbreaks in various countries, particularly in Bangladesh, India, and Malaysia. Unfortunately, no efficient vaccine or drug is available now to combat this baneful virus. NiV employs its nucleocapsid protein for genetic material packaging, which is crucial for viral replication inside the host cells. The small interfering RNAs (siRNAs) can play a central role in inhibiting the expression of disease-causing viral genes by hybridization and subsequent inactivation of the complementary target viral mRNAs through the RNA interference (RNAi) pathway. Therefore, potential siRNAs as molecular therapeutics against the nucleocapsid protein gene of NiV were designed in this study. First, ten prospective siRNAs were identified using the conserved nucleocapsid gene sequences among all available NiV strains collected from various countries. After that, off-target binding, GC (guanine-cytosine) content, secondary structure, binding affinity with the target, melting temperature, efficacy analysis, and binding capacity with the human argonaute protein 2 (AGO2) of these siRNAs were evaluated to predict their suitability. These designed siRNA molecules bear promise in silencing the NiV gene encoding the nucleocapsid protein and thus can alleviate the severity of this dangerous virus. Further *in vivo* experiments are recommended before using these designed siRNAs as alternative and effective molecular therapeutic agents against NiV.

## List of abbreviations

| Acronyms | Full form |
|---|---|
| NiV - | Nipah Virus |
| RNAi | RNA interference |
| siRNA - | Small interfering RNA |
| RISC- | RNA-induced silencing complex |
| Tm - | Melting temperature |
| AGO protein - | Argonaute protein |
| PDB - | Protein Data Bank |
| MUSCLE - | Multiple Sequence Comparison by Log- Expectation. |

(*continued on next column*)

(*continued*)

| | |
|---|---|
| NCBI - | National Center for Biotechnology Information |
| BLAST | Basic Local Alignment Search Tool |
| RMSD - | Root Mean Square Deviation |
| SASA - | Solvent-Accessible Surface Area |
| RMSF | Root Mean Square Fluctuation |
| Rg- | Radius Of Gyration |

* Corresponding author at: Department of Biotechnology and Genetic Engineering, University of Development Alternative, Dhaka 1209, Bangladesh.
** Corresponding author.
*E-mail addresses:* arif.khan@bge.uoda.edu.bd (Md.A. Khan), razu002@du.ac.bd (Md.M. Rahaman).

https://doi.org/10.1016/j.meegid.2022.105310
Received 18 October 2021; Received in revised form 20 May 2022; Accepted 24 May 2022
Available online 28 May 2022

## 1. Introduction

Nipah virus (NiV) is a highly virulent bat-borne zoonotic paramyxovirus that causes fatal encephalitis in humans. NiV, a declared global health priority pathogen by the World Health Organization (WHO), has the potential to cause a pandemic due to its zoonotic nature, rapid transmissibility, distribution of the reservoir species (bat) over wide geographic locations, high case fatality along with the unavailability of a vaccine or any other therapeutic agent. Furthermore, mortality rate is high among the infected individuals due to encephalitis and severe respiratory illness (viral pneumonia) (Chua et al., 2000; Satterfield et al., 2016; Luby and Gurley, 2012; Singh et al., 2019). NiV infections in humans have been identified in Malaysia, Singapore, India, Bangladesh, and the Philippines (Hassan et al., 2020; Hauser et al., 2021; Rahman et al., 2021). When it was first detected in Malaysia, in attempts to decipher the natural history of this emerging infectious disease, it was discovered that pigs infected with NiV act as the intermediate hosts. However, fruit bats from the family Pteropodidae are the natural hosts of this deadly virus. First, it was thought that transmission could happen only from direct contact with the secretion of a sick pig or by handling the body parts of a sick animal. However, later it was confirmed that human-to-human transmission can occur equally. Recently, outbreaks in India and Bangladesh have occurred due to eating fruits or drinking unboiled juice of date palm trees contaminated by bats with >75% mortality (Singh et al., 2019; Broder et al., 2013; Luby et al., 2009; Epstein et al., 2020; Rahman et al., 2021). From 2001 to 2014, 248 collective NiV infections were reported in Bangladesh and most of these cases happened from person-to-person transmission (Luby et al., 2009; Hegde et al., 2016; Nikolay et al., 2019).

NiV is categorized as a virus under the *Henipavirus* genus and Paramyxoviridae family. Its genome is approximately 18.2 kb long, and like some other paramyxoviruses, it follows the 'rule of six' in which the total nucleotide number is always a multiple of 6 (Arankalle et al., 2011; Halpin et al., 2004; Harcourt et al., 2005). Thus, six viral genes are included in the NiV genome that encode nine viral proteins. Ribonucleoprotein complex, the core component of a Nipah Virion, is composed of the following- nucleocapsid protein (N), phosphoprotein (P), RNA-dependent RNA polymerase (L), and genomic RNA (Ranadheera et al., 2018).

Here, the nucleocapsid protein-encoding *'N'* gene's role is crucial for viral replication. Encapsidation of NiV genome is achieved with the help of N protein which protects it from being degraded and from the intracellular defense mechanisms of the host. In order to be capable of being used as a template, the viral genome has to be encapsidated. Otherwise, it would lose its competence for the transcription process where RNA-dependent RNA polymerase is required (Ogino and Green, 2019). Thus, the availability of the N protein speeds up viral infection through activation of the replicase enzyme, encapsidation, and regulation of NiV RNA synthesis (Ray et al., 2016). Since NiV infection is associated with a high death rate, there is no approved therapeutic available right now against this virus, and treatment is mainly symptomatic (Nikolay et al., 2019), an immediate invention of antiviral agents against NiV is a demand of the time. In the current study, we have designed siRNAs adopting various bioinformatics tools against the NiV *'N'* gene to silence it and prevent viral proliferation.

RNA interference (RNAi) or post-transcriptional gene silencing is one sort of cellular regulatory mechanism in which an mRNA is forced to be inactivated by being barred from going through the post-transcriptional steps. One effective way of achieving RNA interference is through small interfering RNAs (siRNA) (Levanova and Poranen, 2018). siRNAs are a special kind of RNA that are non-coding double-stranded molecules. They are 21–25 base pairs in length and have a nucleotide sequence of one strand complementary to an mRNA with which the strand binds and ultimately leads to degradation of that mRNA. As a result, specific protein from that specific mRNA is prevented from being translated, and thus the respective gene is silenced (Raja et al., 2019).

Nowadays, siRNA-based treatment is gaining significant contemplation from researchers in cancer, genetic and infectious diseases. siRNA can reduce tumor growth and enhance immune response in mouse melanoma models (Liu et al., 2018). siRNA-based treatment options have also shown promise in treating Alzheimer's and Parkinson's disease, myopathies, viral infections, and many other diseases. Additionally, there has been much improvement in siRNA delivery methods to ensure specificity while reducing toxicity and increasing bioavailability (Seyhan, 2011). More importantly, three siRNA drugs have recently gained approval from the FDA and seven other siRNA drugs are currently under trial (Zhang et al., 2021). Most interestingly, Mungall et al. showed that siRNAs against the *'N'* gene of NiV arrest viral replication *in vitro (*Mungall et al., *2008)*.

Considering the promise of siRNA, in this study we have endeavored to design universal siRNAs against the deadly NiV employing different computational tools. Previously, Oany et al. (Oany et al., 2015) designed siRNAs against the nucleocapsid gene of only 5 Bangladeshi NiV strains. However, we have worked with all currently available strains, our obtained results are more complete, and not limited by any geographical boundary. Furthermore, we have cross-checked them against two databases for efficacy prediction and also checked their binding affinity with human argonaute protein, a step critical for siRNA action, by molecular docking and molecular dynamics simulations.

## 2. Materials and methods

The workflow adopted in this study and the tools used are graphically presented in Fig. 1.

### 2.1. Retrieval of NiV genome sequences

Coding sequences of currently deposited all 60 complete genomes of NiV were first downloaded from the NCBI nucleotide database (https://www.ncbi.nlm.nih.gov/nuccore). This database was searched with the following keywords, "Nipah virus, complete genome." Secondly, coding sequences of nucleocapsid protein-encoding *'N'* gene (here gene should be perceived as mRNA because NiV is a negative-strand RNA virus) were extracted using a Linux computing platform bash script.

### 2.2. Evolutionary divergence study

A phylogenetic tree was constructed with the *'N'* genes to decipher mutations among different strains. At first, the MUSCLE algorithm incorporated in MEGA X software (Kumar et al., 2018) was employed to perform multiple sequence alignment (MSA). Then, from this MSA, a phylogenetic tree was constructed employing the 'Maximum Likelihood Method' with 1000 as the bootstrap value and following Tamura Nei's evolution model (Tamura and Nei, 1993). Finally, the phylogenetic tree was visualized with iTOL (Letunic and Bork, 2021).

### 2.3. Target selection and siRNA designing

It is established that a minimum 19 nucleotides length guide strand of siRNA and its complementary sequence in the target mRNA are required for successful siRNA mediated gene inhibition (Grimm, 2009). Nineteen such sequences with a minimum of 19 nucleotides length were found conserved among all the 60 *'N'* genes and extracted for downstream analyses. siRNAs were designed against the identified 19 nucleotide targets employing the siDirect web server (Naito et al., 2009). This server completes the task in three steps: i) significantly functioning siRNA identification, ii) seed-dependent off-target impacts minimization, and iii) near-perfect matched genes eradication. A combination of rules advised by Ui-Tei (Ui-Tei et al., 2004), Amarzguioui (Amarzguioui and Prydz, 2004), and Reynolds (Reynolds, 2004) were followed (Table 1) during siRNA designing. During the design of the siRNA duplex, melting temperature ($T_m$) was maintained below 21.5 °C (a

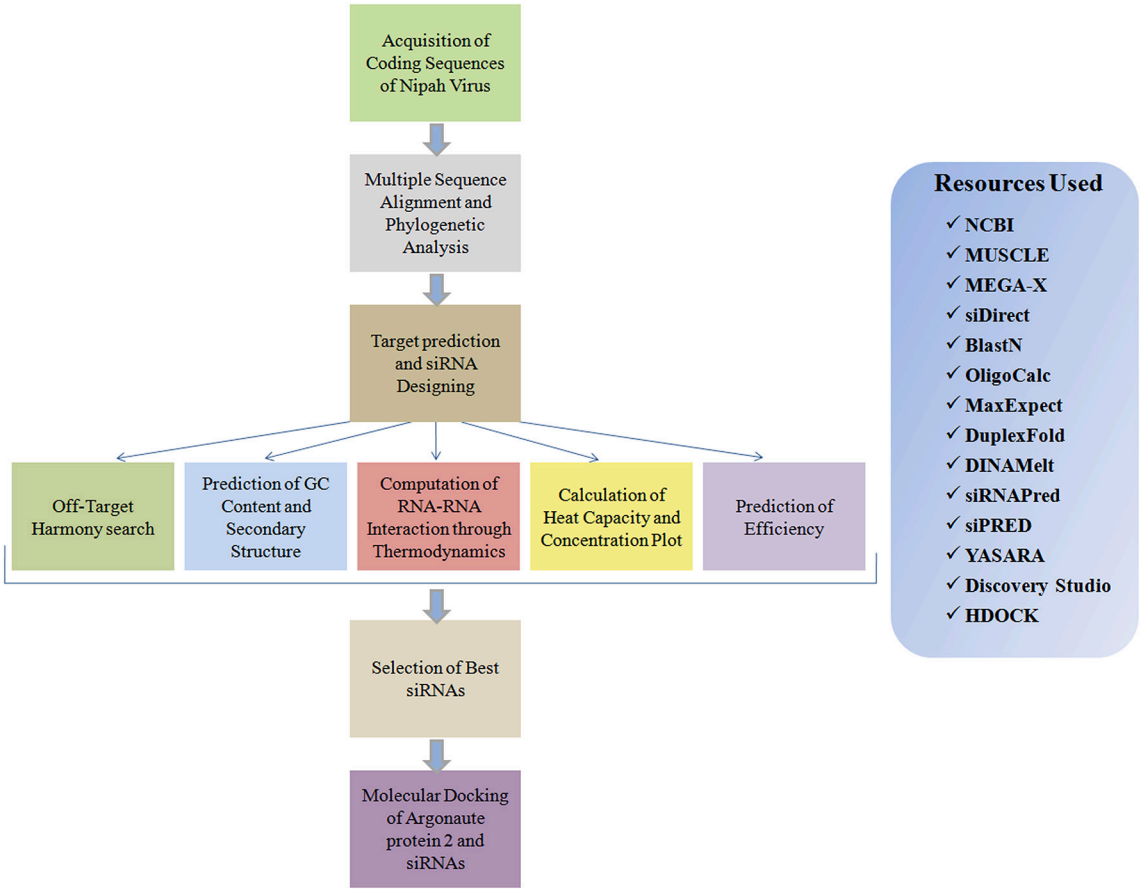


**Fig. 1.** Flowchart describing methodology of the current study.

**Table 1**
Rules followed during designing the siRNA molecules.

| Serial No. | Rules Proposed by | Rule description |
|---|---|---|
| 1 | Ui-Tei et al. (2004) | A or U at the 5′ terminus of the sense strand<br>G or C at the 5′ terminus of the antisense strand<br>At least 4 A or U residues present in the 5′ terminal 7 bp of sense strand<br>GC stretch no longer than 9 nt |
| 2 | Amarzguioui et al. (2004) | Duplex End A or U differential >0<br>No U at position 1<br>Strong binding of 5′ sense strand<br>Presence of A at position 6<br>Weak binding in case of 3′ sense strand |
| 3 | Reynolds et al. (2004) | 1 point for GC content 30–52%<br>1 point for each occurrence of three or more A or U base pairs at position 15–19 of sense strand<br>1 point for little internal stability at target site (Tm > − 20 °C)<br>1 point for occupancy of U at position 10 of the sense strand<br>1 point for occupancy of A at position 3 of the sense strand<br>1 point for occupancy of A at position 19 of the sense strand<br>1 point for Absence of G at position 13 of the sense strand<br>Threshold for efficient siRNAs score ≥ 6 |

default restraint). It was found that keeping the $T_m$ under this temperature minimizes off-target effects (Ui-Tei et al., 2008). The $T_m$ was computed utilizing the equation below:

$$T_m = (1000*\Delta H)/(A + \Delta S + R\ ln\ (CT/4)) - 273.15 + 16.6\log\ [Na^+]$$

where,

- ΔH (kcal/ mol) represents the sum of the nearest neighbor enthalpy changes
- A represents the helix initiation constant (− 10.8)
- ΔS indicates the sum of the nearest neighbor entropy changes
- R represents the gas constant (1.987 cal/deg./mol)
- CT indicates the total molecular concentration (100 μM) of the strand, and
  [$Na^+$] represents the sodium concentration (was fixed to 100 mM).

### 2.4. Off-target binding exploration

A nucleotide BLAST (Camacho et al., 2009) search was run against the 'human genomic plus transcript databases' from the NCBI BLAST suite for identifying possible sequences in the human genome that may face unexpected off-target inhibition. The expected threshold value (*E*-value) was set to 1000 to detect exact complementary off-targets.

### 2.5. Calculation of GC content & prediction of secondary structures of the siRNA guide strands

GC content is an essential regulator of siRNA efficacy (Safari et al., 2017). The Amount of GC content found in the predicted siRNAs was calculated by OligoCalc (Kibbe, 2007). MaxExpect, a program of RNA structure suite (https://rna.urmc.rochester.edu/RNAstructureWeb/Ser

vers/MaxExpect/MaxExpect.html), was used to estimate the secondary structures of the siRNA guide strands (Bellaousov et al., 2013). MaxExpect calculates 'Energy Score' for every query, indicating a predicted structure's favorability.

### 2.6. siRNA- target mRNA binding affinity prediction based on thermodynamics

Target mRNA - guide strand of siRNA complex indicates enhanced silencing activity if a high binding affinity is observed between them. Binding affinity between each target and the corresponding siRNA guide strand was predicted from their thermodynamic interactions by DuplexFold (Piekna-Przybylska et al., 2010).

### 2.7. siRNA-mRNA complex melting temperature prediction

DINAMelt webserver (Markham and Zuker, 2005) was used for the prediction of melting temperatures of the siRNA-mRNA complexes. DINAMelt conducts different calculations for such predictions. A heat capacity plot calculated by DINAMelt exhibits individual contributions of the components to the ensemble heat capacity. This type of heat capacity ($C_p$) is attained as a function of temperature. Heat capacity-melting temperature, $T_m$ ($C_p$) is indicated by the local maximum of the heat capacity curve. Moreover, concentration-melting temperature, $T_m$ (Conc.) is determined as the value at which the concentration of a double-strand molecule (*e.g.*, siRNA-mRNA complex) becomes halved of its initial maximum value. $T_m$ (Conc.) of the siRNA-mRNA complexes were also calculated and visualized *via* a concentration plot.

### 2.8. Efficacy prediction of designed siRNAs

Two large databases named siRNAPred (Kumar et al., 2009) and siPred (Pan and Chen, 2011) were employed to predict the efficacy of the designed siRNAs. Hybrid-7 prediction approach was chosen to evaluate the predicted siRNAs against the primary 21 datasets of siRNAPred. A siRNAPred score greater than 1 suggests "very high" effectiveness, while a score in 0.8–0.9 range suggests "high effectiveness". Again, a score ranging 0.7–0.8 suggests "moderate effectiveness". A siPred inhibition efficacy score higher than 80% is desired.

### 2.9. Molecular docking of siRNAs with human argonaute protein

The binding of siRNA with argonaute (AGO) protein is a crucial step in siRNA-mediated gene silencing. siRNA first becomes a part of RNA-Induced Silencing Complex (RISC) of which AGO proteins are members. Human argonaute protein family includes eight members. AGO 1–4 can load miRNAs and siRNAs. However, only argonaute-2 (AGO2) possesses endonuclease activity. Once the siRNA finds and attaches to the target mRNA, AGO2 cleaves the target mRNA sequence (Meister et al., 2004). To see how our designed siRNAs would bind to AGO2, we docked them against the AGO2 siRNA binding site. First, the crystal structure of human argonaute-2 bound to a siRNA (PDB ID: 5JS1) was collected from the RCSB Protein Data Bank. Then, the AGO 2 protein was cleaned using Discovery Studio Visualizer (version 20.1). After that, the YASARA force field was applied to minimize energy of the protein structure. 3D structures of the siRNA guide strands were obtained employing RNAComposer (http://rnacomposer.cs.put.poznan.pl/). Next, they were optimized in Avogadro (version 1.1.1) employing the MMFF94 force field. One thousand steps and 10e-7 as the convergence value were chosen during optimization to maintain the Steepest Descent algorithm. Finally, HDOCK server (http://hdock.phys.hust.edu.cn/) was utilized for performing molecular docking studies of the siRNA guide strands against the AGO2 protein. During docking, the binding site was defined as the regions that encompass the residues of AGO2 that bind to the siRNA. Binding site residue information was curated from the UniProt database (https://www.uniprot.org/uniprot/Q9UKV8). HDOCK calculated 10 binding modes of each siRNA and the siRNA-AGO2 complex with the lowest docking score was considered as the best binding pose for each siRNA.

### 2.10. Molecular dynamics simulation

RNAComposer predicted the 3D structures of our guide siRNA strands. However, in doing so, it also designed possible internal loops in some of the 3D structures. siRNAs that bind to AGO proteins usually do not bear any loop, and from the analyses of other tools, we have found that the chance of loop formation in our designed siRNAs is low. Considering these conditions, we chose the 4E siRNA-AGO2 complex for molecular dynamics study for the following reasons: i) the siRNA does not have an internal loop in the three-dimensional structure in this complex and ii) the score obtained after docking is also the least negative among similar other complexes (where the siRNA does not have a loop in its 3D structure). We postulated that if the results of molecular dynamics simulation of this complex come satisfactory, we can extrapolate stability of other complexes from these results. With the support of AMBER14 force field, the molecular dynamics study was conducted in YASARA dynamics software package (Land and Humble, 2018; Wang et al., 2004). After initial cleaning and optimization of the docked complex, the hydrogen bond networks were oriented. A cubic simulation cell was generated where the TIP3P solvation model maintained periodic boundary conditions (Harrach and Drossel, 2014). Then, a constant value of acid dissociation was calculated for all the amino acids present in the protein. The actual protonation state of each amino acid residue was maintained by the SCWRL algorithm and hydrogen bond network optimization (Krieger et al., 2012). The physiological conditions of the simulation cell were maintained by setting the pH at 7.4, temperature at 310 K, and NaCl concentration at 0.9% (Krieger et al., 2006). In order to minimize the energy of the complex, the simulated annealing method was applied with the steepest gradient approach (5000 cycles). The time step for this system was set to 2.0 fs. With a cut-off radius of 8 Å, the Particle Mesh Ewalds (PME) method was used for calculating long-range electrostatic interactions (Essmann et al., 1995). The trajectories of MD simulation were saved after 100 ps and maintaining constant pressure and Berendsen thermostat, the simulation was run for 100 ns (Krieger and Vriend, 2015). To calculate root mean square deviation (RMSD), root means square fluctuation (RMSF), radius of gyration (Rg), solvent accessible surface area (SASA), and the number of hydrogen bonds these trajectories were used.

All simulation trajectories were further subjected to MM-PBSA binding free energy calculation by the YASARA Dynamics software package utilizing the following formula (Mitra and Dash, 2018):

$$\text{Binding Energy} = E_{potRecept} + E_{solvRecept} + E_{potLigand} + E_{solvLigand} - E_{potComplex} - E_{solvComplex}$$

Here, YASARA built-in macros were used to calculate MMPBSA binding energy using AMBER 14 force field, where more positive energies indicate better binding between molecules (Srinivasan and Rajasekaran, 2016).

## 3. Results

### 3.1. Evolutionary divergence study, target selection, and siRNA devising

Nineteen conserved sequences were found through multiple sequence alignment of 60 coding sequences of NiV nucleocapsid protein gene (Supplementary file 1). Later, using these sequences, a phylogenetic tree was constructed in which a few sequences exhibited noticeable divergence (>70% bootstrap value) (Fig. 2). This outcome suggests that most of the Nipah virus nucleocapsid gene sequences are conserved and thus could be utilized to create siRNAs against them that would target an extensive range of strains.

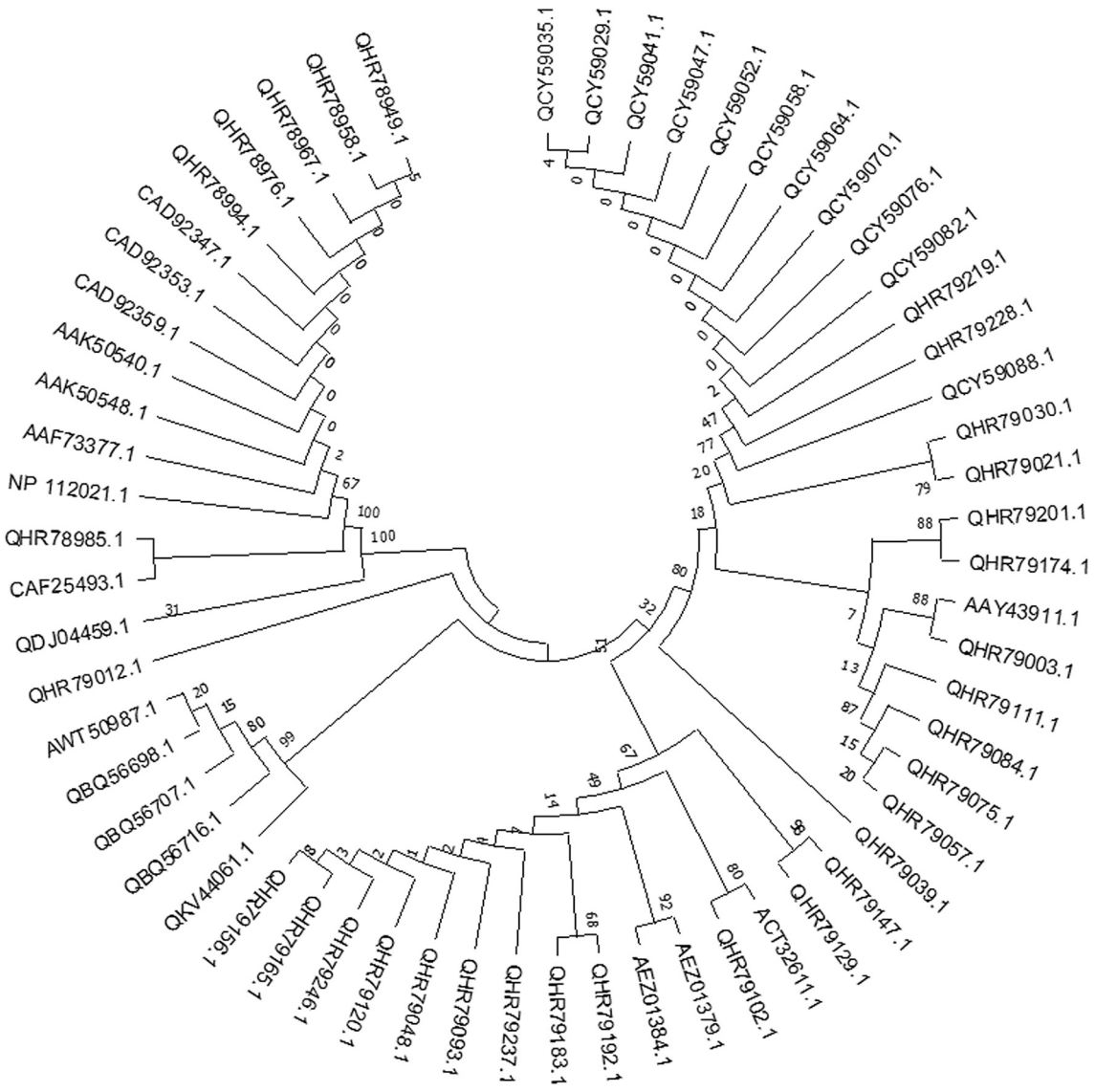


**Fig. 2.** Phylogenetic tree of the nucleocapsid gene as obtained from 60 strains of Nipah virus. Tamura-Nei model of evolution and 1000 bootstrap value were used to construct this tree.

For the 19 conserved sequences, finally ten siRNAs were derived using the siDirect webserver (Table 2). The predicted siRNAs have a low seed duplex stability value ($T_m$) (<21.5 °C), indicating that they can avoid non-specific binding (Table 2).

### 3.2. Off-target binding exploration

The BLASTn search against the human genome and transcriptome found no off-target matches. This implies that the siRNAs possibly would not interact anywhere else than with the desired viral targets.

### 3.3. Calculation of GC content & analysis of secondary structures of the siRNA guide strands

The predicted siRNAs have a GC content ranging from 29 to 45% (Table 3). Besides, the siRNA guide strands' secondary structures were also generated and visualized (Fig. 3) by MaxExpect. MaxExpect 'Energy Score' varies between 1.4–2 for these siRNAs (Table 3).

### 3.4. siRNA- target mRNA binding affinity prediction based on thermodynamics

The free energies of binding between the target NiV mRNAs and their counterpart siRNA guide strands were computed. The range of these values spanned from −38.8 to −30.1 kcal/mol for the ten predicted siRNAs (Table 3 & Fig. 4). These data demonstrate superior interaction capacity of these siRNAs.

### 3.5. siRNA-mRNA complex melting temperature prediction

Melting temperatures of the siRNA-mRNA complexes were calculated in two ways: $T_m$ ($C_p$) and $T_m$ (Conc.). The greater these two melting temperatures are, the more influential the corresponding siRNA is. Values of $T_m$ ($C_p$) span between 80.8 °C and 93.5 °C, and that of $T_m$ (Conc.) vary between 82.8 °C and 92.9 °C (Table 3). For a specific siRNA, these two values show slight difference.

### 3.6. Verification of the predicted siRNA molecules

The effectiveness of the siRNA molecules was evaluated against

**Table 2**
Predicted siRNAs (guide strand + passenger strand) against the nucleocapsid gene of Nipah virus.

| Conserved sequence | siRNA | siRNA Target position in conserved sequence | Target Sequence 21 nt target + 2 nt overhang | siRNAoligo sequences 21 nt guide (5′ → 3′) 21 nt passenger (5′ → 3′) | Seed-duplex stability (Tm) | |
|---|---|---|---|---|---|---|
| | | | | | Guide | Passenger |
| 1 | 1A | 9–31 | TAGGAGTTATCAATCTAAGTTAG | AACUUAGAUUGAUAACUCCUA<br>GGAGUUAUCAAUCUAAGUUAG | 18.9 °C | 14.5 °C |
| 1 | 1B | 10–32 | AGGAGTTATCAATCTAAGTTAGG | UAACUUAGAUUGAUAACUCCU<br>GAGUUAUCAAUCUAAGUUAGG | 9.8 °C | 14.5 °C |
| 2 | | | GCTACTAATAGTCCAGAGCTCAGATGGGAACTAACATT | No effective siRNA candidates were found. | | |
| 3 | | | ACACTCATCTCTATGTATTCAGAGAGACCCGGGGC | No effective siRNA candidates were found. | | |
| 4 | 4A | 3–25 | CCTCAATGACCCAGACATTGAAG | UCAAUGUCUGGGUCAUUGAGG<br>UCAAUGACCCAGACAUUGAAG | 20.5 °C | 20.5 °C |
| 4 | 4B | 13–35 | CCAGACATTGAAGCTGTAATAAT | UAUUACAGCUUCAAUGUCUGG<br>AGACAUUGAAGCUGUAAUAAU | 11.6 °C | 20.5 °C |
| 4 | 4C | 14–36 | CAGACATTGAAGCTGTAATAATA | UUAUUACAGCUUCAAUGUCUG<br>GACAUUGAAGCUGUAAUAAUA | 8.5 °C | 20.5 °C |
| 4 | 4D | 15–37 | AGACATTGAAGCTGTAATAATAG | AUUAUUACAGCUUCAAUGUCU<br>ACAUUGAAGCUGUAAUAAUAG | 1.4 °C | 13.8 °C |
| 4 | 4E | 16–38 | GACATTGAAGCTGTAATAATAGA | UAUUAUUACAGCUUCAAUGUC<br>CAUUGAAGCUGUAAUAAUAGA | −8.0 °C | 12.0 °C |
| 5 | | | GAGGAGATGGAAGGCTTGATGAGAAT | No effective siRNA candidates were found. | | |
| 6 | | | CGGATAACAGACATGAGCAC | No effective siRNA candidates were found. | | |
| 7 | | | CAACAAAAGAGAGTCAATCC | No effective siRNA candidates were found. | | |
| 8 | | | GAAGTCAAGAAAGGAGGATCTGCTAAAGGCAGAGCAGT | No effective siRNA candidates were found. | | |
| 9 | | | ATGGCAGGATTCTTCGCAACCATCAGATT | No effective siRNA candidates were found. | | |
| 10 | | | GGGTTGGAGACAAGGTATCCAGCACTTGCACTCAA | No effective siRNA candidates were found. | | |
| 11 | | | GAATTCCAGAGTGACCTCAACACC | No effective siRNA candidates were found. | | |
| 12 | | | AGCTTGATGCTACTCTACAGAGAAATTGG | No effective siRNA candidates were found. | | |
| 13 | 13A | 9–31 | CCCTTATATGGTGCTTCTTGAAG | UCAAGAAGCACCAUAUAAGGG<br>CUUAUAUGGUGCUUCUUGAAG | 16.6 °C | 0.0 °C |
| 13 | 13B | 10–32 | CCTTATATGGTGCTTCTTGAAGA | UUCAAGAAGCACCAUAUAAGG<br>UUAUAUGGUGCUUCUUGAAGA | 20.4 °C | 14.0 °C |
| 13 | 13C | 19–41 | GTGCTTCTTGAAGAATCAATTCA | AAUUGAUUCUUCAAGAAGCAC<br>GCUUCUUGAAGAAUCAAUUCA | 7.2 °C | 16.6 °C |
| 14 | | | ATGGGTGTGGCTACTACTATTGACAGGTCTAT | No effective siRNA candidates were found. | | |
| 15 | | | TTCAGACTAGGCCAAAAATCAGCACGTCACCA | No effective siRNA candidates were found. | | |
| 16 | | | ATCAAGTTGCAGAACTCGCTGC | No effective siRNA candidates were found. | | |
| 17 | | | GAAACATCAGCAGGAAGGCAAGAGAG | No effective siRNA candidates were found. | | |
| 18 | | | AAATTTGCTGCAGGAGGTGTGCT | No effective siRNA candidates were found. | | |
| 19 | | | GGTGGGACCAGATTGACTAATTC | No effective siRNA candidates were found. | | |

siRNAPred and siPRED. siRNApred predicted Efficacy Score ranges from 0.784 to 0.960, except for one siRNA (0.705 for 13B siRNA) (Table 3). In terms of siPRED, Inhibition Efficacy Score span 82.77%–94.80% (Table 3). These values suggest high efficacy of the designed siRNAs. Therefore, all these siRNAs were selected for further molecular docking studies.

### 3.7. Molecular docking of siRNAs with human argonaute protein

The predicted siRNAs were docked with human AGO2 protein. 4D siRNA showed the lowest docking score (−294.98) among the AGO2-siRNA complexes, while 4B siRNA experienced the highest score (−191.11). A more negative docking score is considered more favorable according to the HDOCK algorithm. Other siRNAs have docking scores between these two values (Table 4 & Fig. 5). Moreover, the binding interface residues of each siRNA-AGO2 complex were also identified (Table 4 & Supplementary file 2).

### 3.8. Molecular dynamics simulation

Molecular dynamics simulation was conducted to verify molecular docking results. Fig. 6(a) demonstrates that the RMSD profile rose up to 30 ns. Then, it became stable and maintained similar values until the last phase of the simulation. The whole RMSD profile never exceeded 2.5 Å, and after becoming stable, the RMSD values fluctuated within 0.3 Å. This suggests a very stable status of the complex. The RMSF profile (Fig. 6(b)) indicates that maximum amino acid residues of AGO2 showed an RMSF value <2.5 Å except for ARG126, ARG150, GLN297, GLN298, GLU299, Ser300, GLY301, GLN302, THR303, VAL304, ARG423, ARG460, and ASP838. Their presence in random coil zones can

**Table 3**
Different parameters of the effective siRNAs against the nucleocapsid gene of Nipah virus.

| siRNA | Conserved position in genomic RNA | Location of target in coding sequence | siRNA target within mRNA | GC content (%) | MaxExpect calculated Energy Score | Free energy of binding between target and guide strands (kcal/mol) | Tm (conc.) | Tm (Cp) | siRNApred predicted Efficacy Score (Hybrid-7) | siPRED predicted Inhibition Efficacy |
|---|---|---|---|---|---|---|---|---|---|---|
| 1A | 145–167 | 33–55 | TAGGAGTTATCAATCTAAGTTAG | 31 | 1.7 | −30.7 | 84.3 °C | 85.5 °C | 0.910 | 89.69% |
| 1B | 146–168 | 34–56 | AGGAGTTATCAATCTAAGTTAGG | 31 | 1.7 | −30.8 | 83.1 °C | 84.4 °C | 0.953 | 94.80% |
| 4A | 385–407 | 273–295 | CCTCAATGACCCAGACATTGAAG | 45 | 2.0 | −38.8 | 92.9 °C | 93.5 °C | 0.884 | 82.77% |
| 4B | 395–417 | 283–305 | CCAGACATTGAAGCTGTAATAAT | 33 | 2.0 | −34.3 | 88.5 °C | 89.7 °C | 0.960 | 93.33% |
| 4C | 396–418 | 284–306 | CAGACATTGAAGCTGTAATAATA | 31 | 1.8 | −31.7 | 86.1 °C | 87.4 °C | 0.894 | 91.22% |
| 4D | 397–419 | 285–307 | AGACATTGAAGCTGTAATAATAG | 29 | 1.7 | −30.3 | 84.4 °C | 82.8 °C | 0.861 | 88.63% |
| 4E | 398–420 | 286–308 | GACATTGAAGCTGTAATAATAGA | 29 | 1.7 | −30.1 | 82.8 °C | 80.8 °C | 0.929 | 91.95% |
| 13A | 1036–1058 | 924–946 | CCCTTATATGGTGCTTCTTGAAG | 40 | 2.0 | −36.6 | 91.1 °C | 90.6 °C | 0.784 | 84.50% |
| 13B | 1037–1059 | 925–947 | CCTTATATGGTGCTTCTTGAAGA | 36 | 1.9 | −34.2 | 89.9 °C | 89.9 °C | 0.705 | 82.97% |
| 13C | 1046–1068 | 934–956 | GTGCTTCTTGAAGAATCAATTCA | 33 | 1.4 | −30.9 | 85.3 °C | 85.9 °C | 0.786 | 88.26% |

explain their high RMSF values. The radius of gyration (Rg) was calculated to determine the compactness of the complex in physiological conditions. A higher Rg value correlates with the flexible nature of the protein-ligand system. This flexibility may arise from the folding and unfolding behavior of the receptor protein. Fig. 6(c) indicates that the Rg profile of the siRNA-AGO2 complex was steady from the very beginning to the last of the simulation time, which confirms satisfactory rigidness. Solvent-accessible surface areas of the complex were also assessed. The SASA profile of the 4E siRNA-AGO2 protein complex (Fig. 6(d)) was stable at the initial phase of the simulation (up to 20 ns time). After that, it started to go upward for ten ns. Then after a peak (41,400Å) at about 30 ns, the SASA value decreased and by 45 ns became stable. This stability was maintained up to the simulation completion with an average SASA value of 40,500 Å. A stable SASA profile suggests the siRNA-AGO2 complex would also be stable inside the body. Fig. 6(e) indicates that the number of hydrogen bonds in the system remained almost identical throughout the simulation period with few variations.

Moreover, binding free energy was also calculated from the simulation trajectories, where a more positive score defines a more favorable binding. Fig. 7 indicates that the 4E siRNA-AGO2 complex exhibited astable binding free energy trend and more positive scores, which define strong interactions in the complex.

## 4. Discussion

In 1998, NiV emerged as a novel fatal virus, inducing unavoidable occurrences of morbidity and mortality in animals and humans (Tan et al., 1999), and the outbreak has become a regular incidence in India and Bangladesh (Ang et al., 2018; Islam et al., 2016). NiV utilizes extremely conserved Ephrin B2 and B3 proteins found in all mammals as its entrance receptor, and thus, it can infect various species, namely pigs, cats, dogs, horses, and humans (Bonaparte et al., 2005; Negrete et al., 2006). Transmission from pigs, horses, and bats to human, and human to human happened considerably in earlier outbreaks (Hauser et al., 2021; Gurley et al., 2007; Hughes et al., 2009). Since fruit bats are widely spread, act as NiV reservoirs, and NiV has been detected in these bats in several countries like Malaysia, Cambodia, Singapore, Thailand, India, Bangladesh, and the Philippines, the risk of an outbreak of this virus in new areas is high (Ang et al., 2018; Yob et al., 2001). However, to date, no vaccine or drug can effectively prevent or treat this infection, and no RNAi-dependent treatment has also been developed (Nikolay et al., 2019; Sharma et al., 2019; Wacharapluesadee et al., 2021). Thus siRNA, a next-generation medicine, may be helpful in this scenario, which is why it is the focus of our current research.

In this study, 19 regions having at least 19 nucleotides length were recognized as conserved in the nucleocapsid gene of all available NiV strains. Ten siRNAs were designed ultimately against 3 conserved sequences (Table 2). To enhance the precision of siRNA prediction, the U, R, A (Ui-Tei, Amarzguioui, and Reynolds) guidelines were followed. In addition, by maintaining the $T_m$ under 21.5 °C, the possibility of siRNA—non-target complex generation was minimized. The GC content of a siRNA influences its performance. Recommended level of GC content in a designed siRNA is 30%–64% (Safari et al., 2017). Our designed ten siRNAs showed GC content in this range except for 4D and 4E (29%).

The formation of internal loops in a siRNA may prevent effective binding and subsequent degradation of the target mRNA sequence. Therefore, it is imperative to unravel the secondary structures of the designed siRNAs and their structural stability. In this study, MaxExpect web server was utilized to anticipate secondary structures of the siRNA guide strands. MaxExpect calculated Energy Scores remained within 2.0, indicating that the siRNAs are stable and can be chosen for effective binding.

The DuplexFold webserver elucidated target and guide strand interactions and related binding energies. A low binding energy suggests a more intimate interaction, and hence a better likelihood of inhibiting the target. All the ten siRNAs have a binding free energy value below −30 kcal/mol (Fig. 4 & Table 3), suggesting that they would interact sufficiently with their related targets. siRNA-mRNA complex melting temperatures were obtained using the DINA Melt web server. Each of the ten siRNA-target mRNA complexes showed a high $T_m$ value (>80 °C) (Table 3). This suggests that the siRNA-target mRNA complexes would be pretty stable in the body temperature.

Inhibitory efficiency of the siRNAs was determined with the help of siRNAPred and siPred web servers. These two programs predict the efficacy of a given siRNA employing machine learning approaches. All the designed siRNAs showed sufficient inhibitory capacity from both analyses (Table 3). From the findings of OligoCalc, MaxExpect, DuplexFold, DINAMelt, siRNAPred, and siPred, it can be expected that these ten

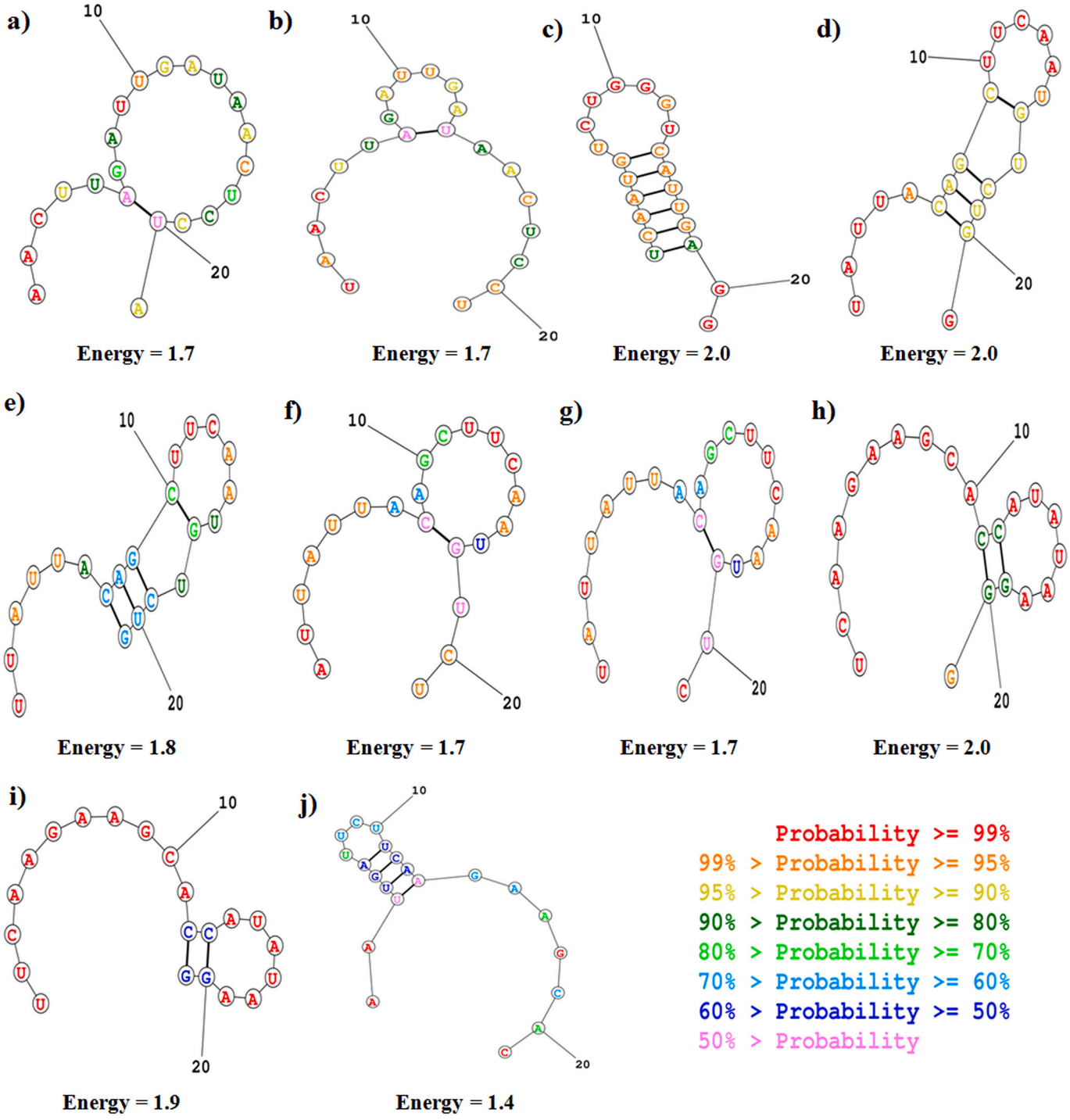


**Fig. 3.** Illustration of secondary structures of ten prospective siRNA guide strands. The structures are indicated as follows: a) 1A, b) 1B, c) 4A, d) 4B, e) 4C, f) 4D, g) 4E, h) 13A, i) 13B, and j) 13C siRNAs.

siRNAs are likely to perform well. However, siRNAs need to bind to the Argonaute protein to perform silencing (Boland et al., 2010; Boland et al., 2011; Müller et al., 2020). Therefore, to further understand the interactions of these siRNAs with the AGO2 protein, the essential enzyme in RISC, molecular docking studies were conducted.

The PDB structure 5JS1, a human AGO2 protein bound to a siRNA, was used to predict siRNA-AGO2 binding employing the HDOCK server. The resultant best docking complexes with their docking scores were retrieved from the server, and the binding residues were also analyzed (Fig. 5, Table 4, Supplementary file 2).

The docking scores of siRNA-AGO2 protein complexes were −191.11 and −294.98 for 4B and 4D, respectively, and the other siRNAs showed docking scores in between them (Table 4). These results suggest that these siRNAs would have a higher potency during RNAi (Kandeel and Kitade, 2013). The 1A siRNA interacts with GLY524, THR526, TYR529, LYS533, GLN548, GLN757, TYR790, ARG792, TYR804, and ARG812 residues of AGO2 (Table 4), which were also reported to interact with siRNAs in previous studies (Bhandare and Ramaswamy, 2016; Elkayam et al., 2012). ASN551, THR559, TYR790, ARG792, and TYR804 are the reported residues of AGO2 bound with the 4D siRNA, which showed the highest binding affinity (lowest docking score) (Table 4). Binding residues of AGO2 in contact with other siRNAs can also be found in Table 4.

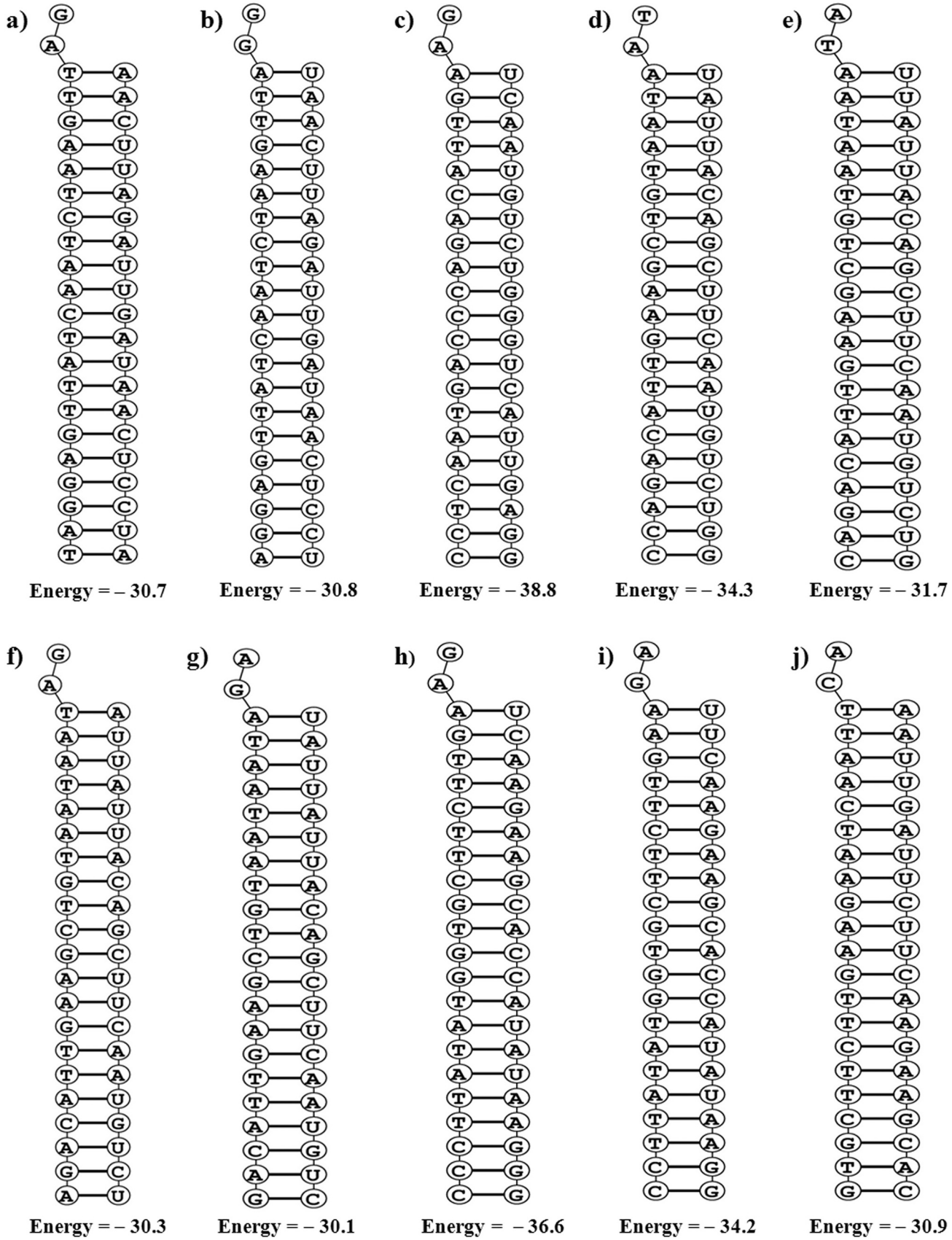


**Fig. 4.** Structures showing the siRNAs (guide strand) bound to their respective targets with relative minimum free energies. These structures are indicated as follows: a) 1A, b) 1B, c) 4A, d) 4B, e) 4C, f) 4D, g) 4E, h) 13A, i) 13B, and j) 13C siRNA guide strands and their corresponding targets.

**Table 4**
Analysis of molecular docking of siRNAs with the human Argonaute2 protein.

| siRNA | Docking score | Binding interface residues of Argonaute2 protein |
|---|---|---|
| 1A | −222.82 | GLY524, THR526, TYR529, LYS533, GLN548, GLN757, TYR790, ARG792, TYR804, ARG812 |
| 1B | −254.27 | GLN548, ASN551,THR559,ARG792, ARG812 |
| 4A | −198.19 | GLY524, GLN548 |
| 4B | −191.11 | GLY524, THR526 |
| 4C | −192.90 | ILE365, THR526, TYR529, GLN548, ASN551 |
| 4D | −294.98 | ASN551, THR559, TYR790, ARG792, TYR804, |
| 4E | −214.06 | HIS271, ARG277, THR526 |
| 13A | −242.26 | HIS271, ARG277, GLY524, THR526, TYR529, GLN548 |
| 13B | −250.48 | HIS271, ARG277, THR526 |
| 13C | −265.56 | GLY524, THR526, TYR529, LYS533, GLN548, ARG812 |

These molecular docking studies provide an insight into the binding of the predicted siRNAs with the human AGO2 protein.

The molecular dynamics simulation study was performed to explore possible structural deviations and rigidness of the 4E siRNA-AGO2 complex. RMSD values of the C-alpha atoms of AGO2 protein were calculated to understand the receptor's flexibility level. RMSF is a measurement of deviation of a protein's amino acid residues from the reference positions. Rg of a simulated complex gives an idea about how well the complex maintains its compactness. An increase in the SASA value indicates an expansion in the surface area of the protein under investigation, whereas a stable SASA value correlates with minor structural deformities. The presence of hydrogen bonds in a protein-ligand complex is an essential player in maintaining the stable nature of the complex. From the molecular dynamics simulation, all the above-calculated parameters were found satisfactory. These suggest that the 4E-siRNA complex would be stable once inside the body and extrapolating from these results, it can be expected that other siRNA-AGO2 complexes would also be stable in the cellular milieu.

Recently, computational studies for designing drugs and siRNAs have gained popularity, because they significantly reduce the initial workload and provide directions for wet lab experiments (Mahfuz et al., 2020, 2021). Such designed siRNAs are now available against human herpes simplex virus (HSV), human respiratory syncytial virus (RSV), Middle East Respiratory Syndrome Coronavirus (MERS-CoV), and Severe acute respiratory syndrome coronavirus 2 (SARS-CoV-2) (Chowdhury et al., 2021; Malekshahi et al., 2016; Nur et al., 2013; Nur et al., 2015). In addition, other research groups have designed siRNAs against

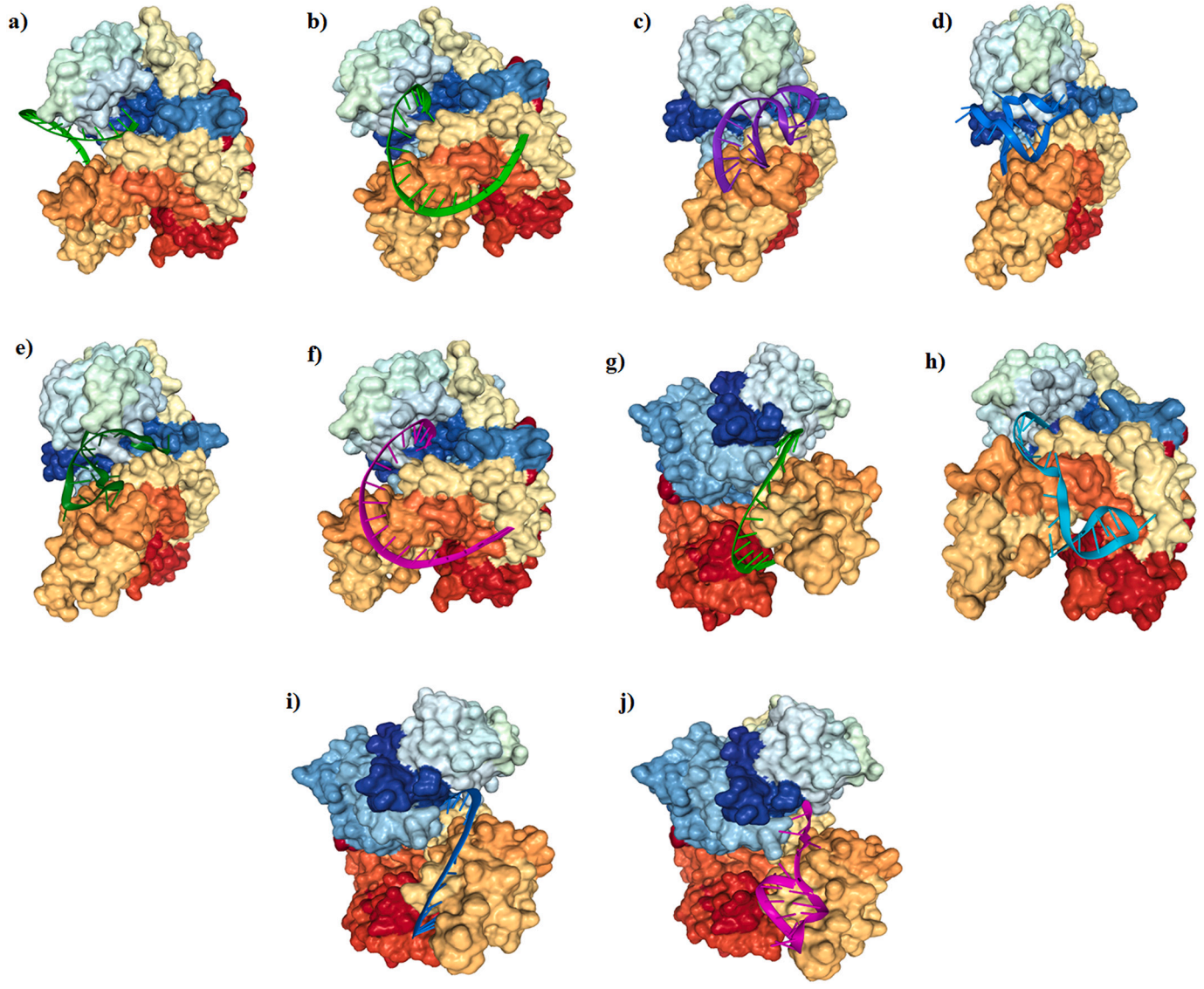


**Fig. 5.** Docked siRNA structures (cartoon view) with human AGO2 protein (surface view). The structures are indicated as follows: a) 1A, b) 1B, c) 4A, d) 4B, e) 4C, f) 4D, g) 4E, h) 13A, i) 13B, and j) 13C siRNA-AGO2 complexes, respectively.

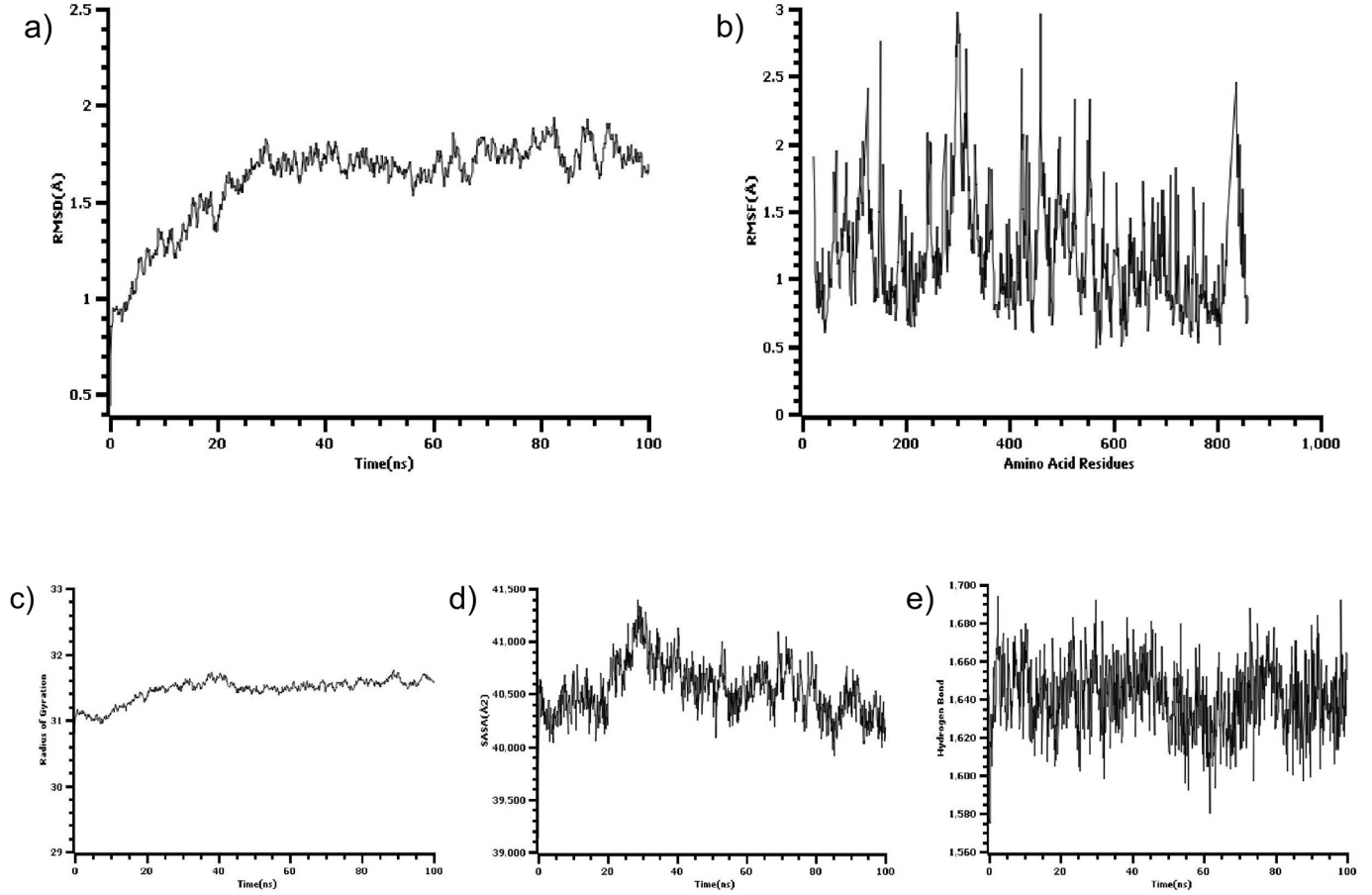


**Fig. 6.** a) RMSD values of the C-alpha atoms of 4E siRNA bound AGO2 residues, b) RMSF values of the C-alpha atoms of 4E siRNA bound AGO2 residues, c) SASA of the amino acid residues of AGO2, d) Rg of AGO2 residues, and e) H-bonds present in the 4E-AGO2 complex.

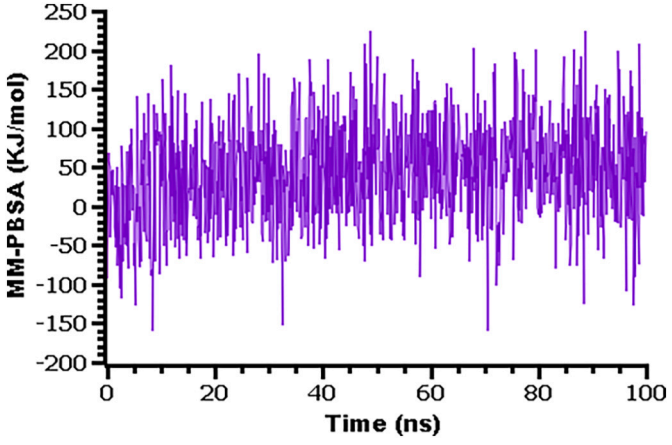


**Fig. 7.** The binding free energy of the 4E siRNA-AGO2 complex derived from molecular dynamics simulation trajectories, where a more positive score defines a more suitable binding.

the Hepatitis C Virus (HCV) and MERS-CoV using computational tools and tested their efficacy *in vitro* on different cell lines (ElHefnawi et al., 2016; Sohrab et al., 2021).

In recent years, many research works have examined a diverse range of *in vivo* usages of siRNAs, either locally or systemically. The majority of these studies have focused on the intravenous delivery of siRNAs. Intranasal and Intravenous delivery of unchanged siRNA molecules into the lungs, which target nucleoproteins of the SARS coronavirus and the influenza virus provide *in vivo* protection against SARS coronavirus fever (Li et al., 2005) and influenza virus complications (Tompkins et al., 2004). Moreover, the use of polyethyleneimine (PEI) for the delivery of RNA, particularly siRNA molecules, has been devised (Urban-Klein et al., 2005). Although chemically unaltered RNAs are volatile and susceptible to degradation, PEI complexation protects RNA molecules from enzymatic and non-enzymatic degradations. In influenza virus infection cases, PEI boosted the delivery of siRNAs into the lungs *via* intravenous route, thus reducing viral growth (Ge et al., 2004). Besides, PEI- siRNA complexes were successfully administered into specific cell types in *in vitro* experiments, and PEI molecules having a low molecular weight showed excellent siRNA protection and transport (Urban-Klein et al., 2005). Under some circumstances, lyophilization protects integrity and functionality of the PEI-RNA complexes (Werth et al., 2006; Brus et al., 2004).

Moreover, siRNA delivery to a specific target and delivery in the desired amount can be achieved using nano vesicles (Gupta et al., 2019). One particular hurdle in NiV infection is crossing the BBB (Blood-Brain Barrier) since NiV causes encephalitis. However, in mice models, siRNAs loaded on different nanoparticles successfully crossed this barrier (Eyford et al., 2021; Zhou et al., 2020; Zou et al., 2020).

## 5. Conclusion

Overall, in this present study, ten potential universal siRNAs were designed to effectively attach and subsequently cleave the nucleocapsid protein-encoding gene of all current NiV strains. Molecular therapeutics may occasionally be ineffective against specific strains. However, our designed siRNAs are likely to address this problem because they target

conserved regions of diverse NiV strains found in different countries. Therefore, these prospective siRNAs can be considered as the most promising molecular therapeutics against the NiV infection. Further extensive *in vitro* studies, studies in suitable laboratory animals, and human trials can prove the actual efficiency of these siRNA molecules.

## Acknowledgement

Md. Arif Khan and Ariful Islam has been partially supported through NIH, National Institute of Allergy and Infectious Diseases (NIAID) Grant #U01AI153420. The funder had no role in study design, data collection and analysis, decision to publish, or preparation of the manuscript.

## CRediT authorship contribution statement

**A.M.U.B. Mahfuz:** Formal analysis, Writing – original draft, Software. **Md. Arif Khan:** Conceptualization, Writing – review & editing, Validation, Supervision. **Emran Hossain Sajib:** Visualization, Software. **Anamika Deb:** Data curation, Writing – original draft. **Shafi Mahmud:** Data curation, Visualization, Software. **Mahmudul Hasan:** Resources, Writing – review & editing. **Otun Saha:** Data curation, Investigation. **Ariful Islam:** Writing – review & editing, Investigation, Validation. **M. Mizanur Rahaman:** Conceptualization, Methodology, Writing – review & editing, Validation.

## Declaration of Competing Interest

The authors declare no conflict of interest for this article. All the authors have read the final version of the manuscript and approved the submission. This original research article has not been submitted or under consideration elsewhere.

## Appendix A. Supplementary data

Supplementary data to this article can be found online at https://doi.org/10.1016/j.meegid.2022.105310.

## References

Amarzguioui, M., Prydz, H., 2004. An algorithm for selection of functional siRNA sequences. Biochem. Biophys. Res. Commun. 316, 1050–1058.
Ang, B.S.P., TCC, Lim, Wang, L., 2018. Nipah virus infection. J. Clin. Microbiol. 56.
Arankalle, V.A., Bandyopadhyay, B.T., Ramdasi, A.Y., Jadi, R., Patil, D.R., Rahman, M., Majumdar, M., Banerjee, P.S., Hati, A.K., Goswami, R.P., 2011. Genomic characterization of nipah virus, West Bengal, India. Emerg. Infect. Dis. 17 (5), 907.
Bellaousov, S., Reuter, J.S., Seetin, M.G., Mathews, D.H., 2013. RNAstructure: web servers for RNA secondary structure prediction and analysis. Nucleic Acids Res. 41, W471–W474.
Bhandare, V., Ramaswamy, A., 2016. Structural dynamics of human argonaute2 and its interaction with siRNAs designed to target mutant tdp43. Adv. Bioinforma. 2016.
Boland, A., Tritschler, F., Heimstädt, S., Izaurralde, E., Weichenrieder, O., 2010. Crystal structure and ligand binding of the MID domain of a eukaryotic Argonaute protein. EMBO Rep. 11, 522–527.
Boland, A., Huntzinger, E., Schmidt, S., Izaurralde, E., Weichenrieder, O., 2011. Crystal structure of the MID-PIWI lobe of a eukaryotic Argonaute protein. Proc. Natl. Acad. Sci. 108 (26), 10466–10471.
Bonaparte, M.I., Dimitrov, A.S., Bossart, K.N., Crameri, G., Mungall, B.A., Bishop, K.A., Choudhry, V., Dimitrov, D.S., Wang, L.-F., Eaton, B.T., 2005. Ephrin-B2 ligand is a functional receptor for Hendra virus and Nipah virus. Proc. Natl. Acad. Sci. 102, 10652–10657.
Broder, C.C., Xu, K., Nikolov, D.B., Zhu, Z., Dimitrov, D.S., Middleton, D., Pallister, J., Geisbert, T.W., Bossart, K.N., Wang, L.-F., 2013. A treatment for and vaccine against the deadly Hendra and Nipah viruses. Antivir. Res. 100 (1), 8–13.
Brus, C., Kleemann, E., Aigner, A., Czubayko, F., Kissel, T., 2004. Stabilization of oligonucleotide–polyethylenimine complexes by freeze-drying: physicochemical and biological characterization. J. Control. Release 95, 119–131.
Camacho, C., Coulouris, G., Avagyan, V., Ma, N., Papadopoulos, J., Bealer, K., Madden, T.L., 2009. BLAST+: architecture and applications. BMC Bioinforma. 10 (1), 1–9.
Chowdhury, U.F., Shohan, M.U.S., Hoque, K.I., Beg, M.A., Siam, M.K.S., Moni, M.A., 2021. A computational approach to design potential siRNA molecules as a prospective tool for silencing nucleocapsid phosphoprotein and surface glycoprotein gene of SARS-CoV-2. Genomics 113, 331–343.
Chua, K., Bellini, W., Rota, P., Harcourt, B., Tamin, A., Lam, S., Ksiazek, T., Rollin, P., Zaki, S., Shieh, W.-J., 2000. Nipah virus: a recently emergent deadly paramyxovirus. Science 288, 1432–1435.
ElHefnawi, M., Kim, T., Kamar, M.A., Min, S., Hassan, N.M., El-Ahwany, E., Kim, H., Zada, S., Amer, M., Windisch, M.P., 2016. In silico design and experimental validation of siRNAs targeting conserved regions of multiple hepatitis C virus genotypes. PLoS One 11, e0159211.
Elkayam, E., Kuhn, C.-D., Tocilj, A., Haase, A.D., Greene, E.M., Hannon, G.J., Joshua-Tor, L., 2012. The structure of human argonaute-2 in complex with miR-20a. Cell 150, 100–110.
Epstein, J.H., Anthony, S.J., Islam, A., Kilpatrick, A.M., Ali Khan, S., Balkey, M.D., Ross, N., Smith, I., Zambrana-Torrelio, C., Tao, Y., Islam, A., Quan, P.L., Olival, K.J., Khan, M.S.U., Gurley, E.S., Hossein, M.J., Field, H.E., Fielder, M.D., Briese, T., Rahman, M., Broder, C.C., Crameri, G., Wang, L.F., Luby, S.P., Lipkin, W.I., Daszak, P., 2020. Nipah virus dynamics in bats and implications for spillover to humans. Proc. Natl. Acad. Sci. U. S. A. 117 (46), 29190–29201.
Essmann, U., Perera, L., Berkowitz, M.L., Darden, T., Lee, H., Pedersen, L.G., 1995. A smooth particle mesh Ewald method.*The*. J. Chem. Phys. 103, 8577–8593.
Eyford, B.A., Singh, C.S., Abraham, T., Munro, L., Choi, K.B., Hill, T., Hildebrandt, R., Welch, I., Vitalis, T.Z., Gabathuler, R., 2021. A nanomule peptide carrier delivers siRNA across the intact blood-brain barrier to attenuate ischemic stroke. Front. Mol. Biosci. 8 (133).
Ge, Q., Filip, L., Bai, A., Nguyen, T., Eisen, H.N., Chen, J., 2004. Inhibition of influenza virus production in virus-infected mice by RNA interference. Proc. Natl. Acad. Sci. 101, 8676–8681.
Grimm, D., 2009. Asymmetry in siRNA design. Gene Ther. 16, 827–830.
Gupta, N., Rai, D.B., Jangid, A.K., Pooja, D., Kulhari, H., 2019. Nanomaterials-based siRNA delivery: routes of administration, hurdles and role of Nanocarriers. In: Nanotechnology in Modern Animal Biotechnology. Springer, pp. 67–114.
Gurley, E.S., Montgomery, J.M., Hossain, M.J., Bell, M., Azad, A.K., Islam, M.R., Molla, M.A.R., Carroll, D.S., Ksiazek, T.G., Rota, P.A., 2007. Person-to-person transmission of Nipah virus in a Bangladeshi community. Emerg. Infect. Dis. 13, 1031.
Halpin, K., Bankamp, B., Harcourt, B.H., Bellini, W.J., Rota, P.A., 2004. Nipah virus conforms to the rule of six in a minigenome replication assay. J. Gen. Virol. 85, 701–707.
Harcourt, B., Lowe, L., Tamin, A., Liu, X., Bankamp, B., Bowden, N., Rollin, P., Comer, J., Ksiazek, T., et al., 2005. Genetic Characterization of Nipah Virus, Bangladesh, 2004, pp. 1594–1597.
Harrach, M.F., Drossel, B., 2014. Structure and dynamics of TIP3P, TIP4P, and TIP5P water near smooth and atomistic walls of different hydroaffinity.*The*. J. Chem. Phys. 140 (174501).
Hassan, M.M., Kalam, M.A., Alam, M., Shano, S., Faruq, A.A., Hossain, M.S., Islam, M.N., Khan, S.A., Islam, A., 2020. Understanding the community perceptions and knowledge of bats and transmission of Nipah virus in Bangladesh. Animals 10 (10), 1814.
Hauser, N., Gushiken, A.C., Narayanan, S., Kottilil, S., Chua, J.V., 2021. Evolution of Nipah virus infection: past, present, and future considerations. Trop. Med. Infect Dis. 6 (1), 24.
Hegde, S.T., Sazzad, H.M.S., Hossain, M.J., Alam, M.-U., Kenah, E., Daszak, P., et al., 2016. Investigating rare risk factors for Nipah virus in Bangladesh: 2001–2012. EcoHealth. 13, 720–728. https://doi.org/10.1007/s10393-016-1166-0.
Hughes, J.M., Wilson, M.E., Luby, S.P., Gurley, E.S., Hossain, M.J., 2009. Transmission of human infection with Nipah virus. Clin. Infect. Dis. 49, 1743–1748.
Islam, M.S., Sazzad, H.M., Satter, S.M., Sultana, S., Hossain, M.J., Hasan, M., Rahman, M., Campbell, S., Cannon, D.L., Ströher, U., 2016. Nipah virus transmission from bats to humans associated with drinking traditional liquor made from date palm sap, Bangladesh, 2011–2014. Emerg. Infect. Dis. 22, 664.
Kandeel, M., Kitade, Y., 2013. Computational analysis of siRNA recognition by the Ago2 PAZ domain and identification of the determinants of RNA-induced gene silencing. PLoS One 8, e57140.
Kibbe, W.A., 2007. OligoCalc: an online oligonucleotide properties calculator. Nucleic Acids Res. 35, W43–W46.
Krieger, E., Vriend, G., 2015. New ways to boost molecular dynamics simulations. J. Comput. Chem. 36, 996–1007.
Krieger, E., Nielsen, J.E., Spronk, C.A., Vriend, G., 2006. Fast empirical pKa prediction by Ewald summation. J. Mol. Graph. Model. 25, 481–486.
Krieger, E., Dunbrack, R.L., Hooft, R.W., Krieger, B., 2012. Assignment of protonation states in proteins and ligands: combining pK a prediction with hydrogen bonding network optimization. In: Computational Drug Discovery and Design. Springer, pp. 405–421.
Kumar, M., Lata, S., Raghava, G., 2009. siRNApred: SVM based method for predicting efficacy value of siRNA. In: Proceedings of the first international conference on Open Source for Computer Aided Drug Discovery (OSCADD). CSIR-IMTECH.
Kumar, S., Stecher, G., Li, M., Knyaz, C., Tamura, K., 2018. MEGA X: molecular evolutionary genetics analysis across computing platforms. Mol. Biol. Evol. 35 (1547).
Land, H., Humble, M.S., 2018. YASARA: a tool to obtain structural guidance in biocatalytic investigations. In: Protein Engineering. Springer, pp. 43–67.
Letunic, I., Bork, P., 2021. Interactive tree of life (iTOL) v5: an online tool for phylogenetic tree display and annotation. Nucleic Acids Res. 49 (W1), W293–W296.
Levanova, A., Poranen, M.M., 2018. RNA interference as a prospective tool for the control of human viral infections. Front. Microbiol. 9 (2151).
Li, B.-j., Tang, Q., Cheng, D., Qin, C., Xie, F.Y., Wei, Q., Xu, J., Liu, Y., 2005. Zheng B-j, Woodle MC: using siRNA in prophylactic and therapeutic regimens against SARS coronavirus in Rhesus macaque. Nat. Med. 11, 944–951.

Liu, D.-q., Lu, S., Zhang, L.-x., Ji, M., Liu, S.-y., Wang, S.-W., Liu, R.-T., 2018. An indoleamine 2, 3-dioxygenase siRNA nanoparticle-coated and Trp2-displayed recombinant yeast vaccine inhibits melanoma tumor growth in mice. J. Control. Release 273, 1–12.
Luby, S.P., Gurley, E.S., 2012. Epidemiology of henipavirus disease in humans. Henipavirus 25–40.
Luby, S.P., Hossain, M., Gurley, E.S., Ahmed, B., Banu, S., Khan, S., Rahman, M., 2009. Recurrent zoonotic transmission of Nipah virus into humans, Bangladesh, 2001–2007. Emerg. Infect. Dis. 15 (8), 1229–1235.
Mahfuz, A.M.U.B., Stambuk Opazo, F., Aguilar, L.F., Iqbal, M.N., 2020. Carfilzomib as a potential inhibitor of NADH-dependent enoyl-acyl carrier protein reductases of *Klebsiella pneumoniae* and *mycobacterium tuberculosis* as a drug target enzyme: insights from molecular docking and molecular dynamics. J. Biomol. Struct. Dyn. 1–17.
Mahfuz, A.M.U.B., Iqbal, M.N., Opazo, F.S., Zubair-Bin-Mahfuj, A.M., 2021. Characterization of ribonucleotide reductases of emerging pathogens *Elizabethkingia anophelis* and *Elizabethkingia meningoseptica* and streptonigrin as their inhibitor: a computational study. J. Biomol. Struct. Dyn. 1–13.
Malekshahi, S.S., Arefian, E., Salimi, V., Azad, T.M., Yavarian, J., 2016. Potential siRNA molecules for nucleoprotein and M2/L overlapping region of respiratory syncytial virus: In silico design. Jundishapur J. Microbiol. 9.
Markham, N.R., Zuker, M., 2005. DINAMelt web server for nucleic acid melting prediction. Nucleic Acids Res. 33, W577–W581.
Meister, G., Landthaler, M., Patkaniowska, A., Dorsett, Y., Teng, G., Tuschl, T., 2004. Human Argonaute2 mediates RNA cleavage targeted by miRNAs and siRNAs. Mol. Cell 15, 185–197.
Mitra, S., Dash, R., 2018. Structural dynamics and quantum mechanical aspects of shikonin derivatives as CREBBP bromodomain inhibitors. J. Mol. Graph. Model. 83, 42–52.
Müller, M., Fazi, F., Ciaudo, C., 2020. Argonaute proteins: from structure to function in development and pathological cell fate determination. Front. Cell Dev. Biol. 7, 360.
Mungall, B.A., Schopman, N.C., Lambeth, L.S., Doran, T.J., 2008. Inhibition of Henipavirus infection by RNA interference. Antivir. Res. 80 (3), 324–331. https://doi.org/10.1016/j.antiviral.2008.07.004.
Naito, Y., Yoshimura, J., Morishita, S., Ui-Tei, K., 2009. siDirect 2.0: updated software for designing functional siRNA with reduced seed-dependent off-target effect. BMC Bioinforma. 10, 1–8.
Negrete, O.A., Wolf, M.C., Aguilar, H.C., Enterlein, S., Wang, W., Mühlberger, E., Su, S. V., Bertolotti-Ciarlet, A., Flick, R., Lee, B., 2006. Two key residues in ephrinB3 are critical for its use as an alternative receptor for Nipah virus. PLoS Pathog. 2, e7.
Nikolay, B., Salje, H., Hossain, M.J., Khan, A.D., Sazzad, H.M., Rahman, M., Daszak, P., Ströher, U., Pulliam, J.R., Kilpatrick, A.M., 2019. Transmission of Nipah virus—14 years of investigations in Bangladesh. N. Engl. J. Med. 380, 1804–1814.
Nur, S.M., Al Amin, M., Alam, R., Hasan, M.A., Hossain, M.A., Mannan, A., 2013. An in silico approach to design potential siRNA molecules for ICP22 (US1) gene silencing of different strains of human herpes simplex 1. J. Young Pharmacists 5, 46–49.
Nur, S.M., Hasan, M.A., Al Amin, M., Hossain, M., Sharmin, T., 2015. Design of potential RNAi (miRNA and siRNA) molecules for middle east respiratory syndrome coronavirus (MERS-CoV) gene silencing by computational method. Interdiscip. Sci. Comput. Life Sci. 7, 257–265.
Oany, A.R., Hossain, M.U., Ahmad, S.A.I., 2015. Computational approach to design a potential siRNA molecule to silence the Nucleocapsid gene of different Nipah virus strains of Bangladesh. Biores. Commun. 1 (1), 40–44.
Ogino, T., Green, T.J., 2019. RNA synthesis and capping by non-segmented negative strand RNA viral polymerases: Lessons from a prototypic virus. Front. Microbiol. 10, 1490.
Pan, W.-J., Chen, C.-W., 2011. Chu Y-W: siPRED: predicting siRNA efficacy using various characteristic methods. PLoS One 6, e27602.
Piekna-Przybylska, D., DiChiacchio, L., Mathews, D.H., Bambara, R.A., 2010. A sequence similar to tRNA 3 Lys gene is embedded in HIV-1 U3–R and promotes minus-strand transfer. Nat. Struct. Mol. Biol. 17 (83).
Rahman, M.Z., Islam, M.M., Hossain, M.E., Rahman, M.M., Islam, A., Siddika, A., Hossain, M.S.S., et al., 2021. Genetic diversity of Nipah virus in Bangladesh. Int. J. Infect. Dis. 102, 144–151.
Raja, M.A.G., Katas, H., Amjad, M.W., 2019. Design, mechanism, delivery and therapeutics of canonical and Dicer-substrate siRNA. Asian J. Pharmaceut. Sci. 14, 497–510.
Ranadheera, C., Proulx, R., Chaiyakul, M., Jones, S., Grolla, A., Leung, A., Rutherford, J., Kobasa, D., Carpenter, M., Czub, M., 2018. The interaction between the Nipah virus nucleocapsid protein and phosphoprotein regulates virus replication. Sci. Rep. 8, 1–14.
Ray, G., Schmitt, P.T., Schmitt, A.P., 2016. C-terminal DxD-containing sequences within paramyxovirus nucleocapsid proteins determine matrix protein compatibility and can direct foreign proteins into budding particles. J. Virol. 90, 3650–3660.
Reynolds, A., 2004. Leake D, Boese Q, Scaringe S, Marshall WS, Khvorova a. Rational siRNA design for RNA interference. Nat. Biotechnol. 22, 326–330.
Safari, F., Barouji, S.R., Tamaddon, A.M., 2017. Strategies for improving siRNA-induced gene silencing efficiency. Adv. Pharmaceut. Bull. 7 (603).
Satterfield, B.A., Dawes, B.E., Milligan, G.N., 2016. Status of vaccine research and development of vaccines for Nipah virus. Vaccine 34, 2971–2975.
Seyhan, A.A., 2011. RNAi: a potential new class of therapeutic for human genetic disease. Hum. Genet. 130, 583–605.
Sharma, V., Kaushik, S., Kumar, R., Yadav, J.P., Kaushik, S., 2019. Emerging trends of Nipah virus: a review. Rev. Med. Virol. 29 (e2010).
Singh, R.K., Dhama, K., Chakraborty, S., Tiwari, R., Natesan, S., Khandia, R., Munjal, A., Vora, K.S., Latheef, S.K., Karthik, K., 2019. Nipah virus: epidemiology, pathology, immunobiology and advances in diagnosis, vaccine designing and control strategies–a comprehensive review. Vet. Q. 39, 26–55.
Sohrab, S.S., El-Kafrawy, S.A., Mirza, Z., Hassan, A.M., Alsaqaf, F., Azhar, E.I., 2021. In silico prediction and experimental validation of siRNAs targeting ORF1ab of MERS-CoV in Vero cell line. Saudi J. Biol. Sci. 28, 1348–1355.
Srinivasan, E., Rajasekaran, R., 2016. Computational investigation of curcumin, a natural polyphenol that inhibits the destabilization and the aggregation of human SOD1 mutant (Ala4Val). RSC Adv. 6, 102744–102753.
Tamura, K., Nei, M., 1993. Estimation of the number of nucleotide substitutions in the control region of mitochondrial DNA in humans and chimpanzees. Mol. Biol. Evol. 10, 512–526.
Tan, K.-S., Tan, C.T., Goh, K.J., 1999. Epidemiological aspects of Nipah virus infection. Neurol J. Southeast Asia 4, 77–81.
Tompkins, S.M., Lo, C.-Y., Tumpey, T.M., Epstein, S.L., 2004. Protection against lethal influenza virus challenge by RNA interference in vivo. Proc. Natl. Acad. Sci. 101, 8682–8686.
Ui-Tei, K., Naito, Y., Takahashi, F., Haraguchi, T., Ohki-Hamazaki, H., Juni, A., Ueda, R., Saigo, K., 2004. Guidelines for the selection of highly effective siRNA sequences for mammalian and chick RNA interference. Nucleic Acids Res. 32, 936–948.
Ui-Tei, K., Naito, Y., Nishi, K., Juni, A., Saigo, K., 2008. Thermodynamic stability and Watson–Crick base pairing in the seed duplex are major determinants of the efficiency of the siRNA-based off-target effect. Nucleic Acids Res. 36, 7100–7109.
Urban-Klein, B., Werth, S., Abuharbeid, S., Czubayko, F., Aigner, A., 2005. RNAi-mediated gene-targeting through systemic application of polyethylenimine (PEI)-complexed siRNA in vivo. Gene Ther. 12, 461–466.
Wacharapluesadee, S., Ghai, S., Duengkae, P., et al., 2021. Two decades of one health surveillance of Nipah virus in Thailand. One Health Outlook 3, 12.
Wang, J., Wolf, R.M., Caldwell, J.W., Kollman, P.A., Case, D.A., 2004. Development and testing of a general amber force field. J. Comput. Chem. 25, 1157–1174.
Werth, S., Urban-Klein, B., Dai, L., Höbel, S., Grzelinski, M., Bakowsky, U., Czubayko, F., Aigner, A., 2006. A low molecular weight fraction of polyethylenimine (PEI) displays increased transfection efficiency of DNA and siRNA in fresh or lyophilized complexes. J. Control. Release 112, 257–270.
Yob, J.M., Field, H., Rashdi, A.M., Morrissy, C., van der Heide, B., Rota, P., 2001. Bin Adzhar a, white J, Daniels P, Jamaluddin a: Nipah virus infection in bats (order Chiroptera) in peninsular Malaysia. Emerg. Infect. Dis. 7, 439.
Zhang, M.M., Bahal, R., Rasmussen, T.P., Manautou, J.E., Zhong, X.-B., 2021. The growth of siRNA-based therapeutics: Updated clinical studies. Biochem. Pharmacol. 114432.
Zhou, Y., Zhu, F., Liu, Y., Zheng, M., Wang, Y., Zhang, D., Anraku, Y., Zou, Y., Li, J., Wu, H., 2020. Blood-brain barrier–penetrating siRNA nanomedicine for Alzheimer's disease therapy. Sci. Adv. 6, eabc7031.
Zou, Y., Sun, X., Wang, Y., Yan, C., Liu, Y., Li, J., Zhang, D., Zheng, M., Chung, R.S., Shi, B., 2020. Single siRNA nanocapsules for effective siRNA brain delivery and glioblastoma treatment. Adv. Mater. 32 (2000416).